Proceedings of the ASME-JSME-KSME 2011 Joint Fluids Engineering Conference
AJK-Fluids2011
July 24-29, 2011, Hamamatsu, Shizuoka, JAPAN

AJK2011-16002

FLUID FLOW CHARACTERISTICS AROUND A PAIR OF DIAMOND-SHAPED CYLINDERS IN SIDE-BY-SIDE AND TANDEM ARRANGEMENTS

Shuichi TORII
Graduate School of Science and Technology,
Kumamoto University
Kumamoto, JAPAN

Noritugu UEDA
Graduate School of Science and Technology,
Kumamoto University
Kumamoto, JAPAN

Zijie LIN
Graduate School of Science and Technology,
Kumamoto University
Kumamoto, JAPAN

ABSTRACT

The present study deals with unsteady laminar fluid flow phenomena around a pair of diamond-shaped cylinders in free stream. Emphasis is placed on the effects of the Reynolds number, Re, and the ratio of cylinder separation distance to length of diamond-shaped cylinder, s/d, on the flow patterns in side-by-side and tandem arrangements. The Navier-Stokes equations are discretized using finite difference method to determine the time history of velocity vector in the flow field. The Reynolds numbers, Re, is ranged from 30 to 300 and gap spacing, s/d, is varied from 0.0 to 2.5 for side-by-side and 0.0 to 5.0 for tandem, respectively. The results are compared with the experimental results with the aid of flow visualization method. The study discloses that (i) the generations of Karman vortex streets behind the diamond-shaped cylinders are intensified with an increase in the Reynolds number, (ii) the categorized flow patterns in the wake region of the diamond-shaped islands are affected by s/d, and (iii) the vortex shedding frequency in the wake of diamond-shaped cylinders depends on both the gap spacing and the formation of the vortices.

INTRODUCTION

A separating flow over a bluff body creates an unsteady wake downstream of its body in which vortices are shed alternately from each of the downstream trailing edges of the body. This produces a wake containing an asymmetric array of definable eddies, which are referred to as the von Karman vortex street. The vortex shedding occurs at the Reynolds number greater than the transitional value where large-scale organized motion exists within the turbulent wake downstream of the various bluff obstacles. The corresponding numerous numerical and experimental studies are performed on fluid flow transport phenomena.

As for the fluid flow phenomenon behind a pair of bluff bodies in a stream, Yu and Kareem [1] calculated the velocity and pressure fields in the flow around rectangular prisms with different aspect ratios. Kahawita and Wang [2] carried out two-dimensional numerical simulation respect to the Benard-von Karman hydrodynamic instability behind trapezoidal bluff bodies by means of the spline method of fractional steps. They discussed the effects of trapezoidal height and width on the Strouhal number by comparing the numerical results with the experimentally observed behavior. Agrawal et al. [3] investigated the low Reynolds number flow around two square cylinders placed in side-by-side arrangement using the lattice Boltzmann method (LMB) and linear stochastic estimate (LSE). Valencia et al. [4] computed the flow and heat transfer in a plane channel with two square bars in side-by-side arrangement. They disclosed that heat transfer enhancement and flow pattern are strongly dependent of G/d and the channel Reynolds number. Here, G is transverse spacing between the two bars and d is the bar height. As for the experimental fluid flow phenomenon behind a pair of bluff bodies in a stream, Wang and Zhou [5] investigated the flow behind two side-by-side circular cylinders based on laser-illuminated flow-visualization, particle image velocimetry and hot-wire measurement. They classify three different flow regimes by the ratio T/d (T is the center-to-center cylinder spacing and d is the cylinder diameter), i.e., single street, asymmetrical flow and two coupled streets. Akilli et al. [6] studied experimentally the flow around two and three side-by-side circular cylinders of equal diameter in shallow water using the particle image velocimetry (PIV) technique in the range of G/D of 1.0 to 3.0 at Re=5000. They found that the flow structure behind the cylinders is asymmetrical at small gap ratio, i.e., G/D as a result of jet-like flow from both cylinders. As for the flow over two side-by-side normal plates for which the gap ratios are in the range 1.4 - 2.1. Miau et al. [7], for high Reynolds number region, revealed that the addition of artificial disturbance into the free stream promotes gap flow flopping at low gap ratios. Wei and Chang [8] investigated flow characteristics of wake and base-bleed flow downstream of two bluff bodies, with different cross-sectional geometries (circular, square cylinder and flat plate) in side-by-side arrangement.

Meanwhile, as cylinders in a tandem arrangement, the flow field, particularly the drag force is largely dependent on the spacing between two cylinders and the Reynolds number

[9]. Ohmi and Imaichi [10] disclosed that there is a distinct difference in the flow patterns between the spacing of 3.0 and 5.0 diameters at the Reynolds number of 100. The corresponding numerical simulation at small Reynolds numbers of about 100 - 200 analyzed the effect of the critical spacing on the flow pattern [11-14]. It is disclosed that the flow pattern may intermittently switch between two stable modes, i.e., the reattachment flow and the jump flow, which are affected by the spacing of two square cylinders. That is, the reattachment mode shows reattachment of the separated shear layers from the upstream cylinder to the surface of the downstream cylinder, and the jump mode displays shedding of vortices within the gap between the cylinders. Carmo and Meneghini [15] dealt with the incompressible flow around pairs of circular cylinders in tandem arrangement. Two- and three-dimensional simulation of the flow was carried out in the Reynolds number region of 160 to 320 and in the range of center-to-center distance of 1.5 to 8 diameters. They found that the presence of three-dimensional structures in the flow varies in the interference regime.

Umeda et al. [16] measured the turbulence intensity and Reynolds stresses around a square or diamond-shaped cylinder using two-dimensional laser Doppler velocimetry (LDV). They reported that the vortex appears in the wake flows behind the cylinder for various depth and width of duct. To the authors' knowledge, there is no information on the fluid-flow phenomenon around a pair of diamond-shaped cylinders placed side-by-side or tandem in free stream.

The present study deals with unsteady laminar fluid flow phenomena over two-dimensional twin diamond-shaped islands (i.e. cylinders) in cross flow. Emphasis is placed on the effects of the Reynolds number, Re, and the ratio of cylinder separation distance to length of diamond-shaped cylinder, s/d, on the flow patterns in side-by-side and tandem arrangements. A numerical method is employed to determine velocity profiles over twin diamond-shaped islands. The numerical results are compared with the experimental results with the aid of the flow visualization method.

NUMERICAL METHOD AND EXPERIMENTAL APPARATUS

Consider an unsteady two-dimensional flow over twin diamond-shaped islands placed in side-by-side or tandem arrangement in free stream. The physical configuration and the coordinate system of the flow, for each arrangement are shown in Figs. 1(a) and (b), respectively. The computational field considered here and data output portion are illustrated in Figs. 2(a) and (b), respectively. The positions P_1 and P_2 are located at x/d = 1.5 and y/d = ± (d+s)/2 behind twin cylinders for the side-by-side arrangement and at x/d = 1.5, 2.5+s/d and y/d = 0.0 behind twin cylinders for tandem arrangement. The other positions P_3, P_4, P_5, and P_6 are also shown in Fig. 2.

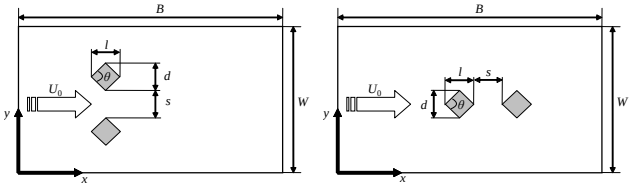

(I) Side-by-side arrangement (II) Tandem arrangement

FIGURE 1. COORDINATE SYSTEM AND COMPUTATIONAL DOMAIN

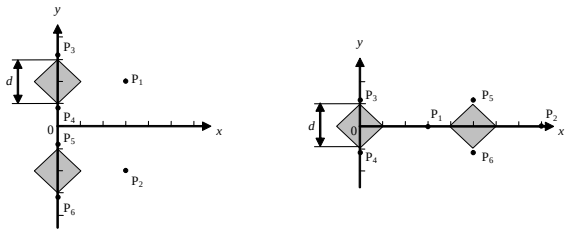

(I) Side-by-side arrangement (II) Tandem arrangement

FIGURE 2. DATA OUTPUT POSITIONS

The following assumptions are imposed in the formulation of the problem based on the flow characteristics considered here: incompressible, laminar flow with constant fluid properties, uniform inlet velocity and uniform inlet fluid temperature in the upstream region. Then the governing differential equations for mass and momentum can be expressed as:

$$\partial u/\partial x + \partial v/\partial y = 0 \quad (1)$$

$$\partial u/\partial t + u\partial u/\partial x + v\partial u/\partial y = -1/\rho(\partial P/\partial x) + \nu(\partial^2 u/\partial x^2 + \partial^2 u/\partial y^2) \quad (2a)$$

$$\partial v/\partial t + u\partial v/\partial x + v\partial v/\partial y = -1/\rho(\partial P/\partial y) + \nu(\partial^2 v/\partial x^2 + \partial^2 v/\partial y^2) \quad (2b)$$

Here u, v, ρ, P, t, and ν are the velocities in the x and y direction, density, pressure, time and kinematical viscosity, respectively. B and W are computational domain in the x and y directions, respectively. Note that B and W are taken to be large enough not to affect the numerical results. l and d are diamond cylinder sizes in the x and y directions, respectively and s is separation distance between a pair of diamonds. θ is an aspect upstream apex angle of the diamond.

The governing equations employed here are discretized using the finite difference methods proposed by Harlow and Welch [17] and Hirt et al. [18]. The numerical cord employed here is developed in our laboratory. The system variables P, u and v are calculated with a staggered grid as proposed by Harlow and Welch [18]. A computation reveals a small difference, i.e., maximum 2%, when the grid system is changed from 400×800 to 800×1600. Hence, a grid system of 400×800 with uniformly distributed nodal points is employed in the present study to save computation time. The nonslip boundary

condition is employed on the surface of the diamond cylinders. The assumed infinitely wide flow field is approximated by a finite domain, i.e., *B* X *W* in numerical calculation. Equations (2a) and (2b), for *u* and *v*, are solved subject to the appropriate diamond-shaped island boundary conditions as:

$u = U_0$, $v = 0$, at the inlet, i.e., $x = 0$

$\partial u/\partial x = 0$, $\partial v/\partial x = 0$, $P=0$ at $x = B$

$u = U_0$, $v = 0$, $P=0$ at $y = 0$ and W

Numerical computation was performed at time interval Δt = 0.0001 sec using air as the working fluid. The Reynolds numbers, Re, based on U_0, d and kinematical viscosity ν is ranged from 30 to 300 for θ=90° and the ratio of cylinder separation distance to length of diamond-shaped cylinder, s/d, is varied from 0.0 to 5.0.

Simulations with various different grids, as mentioned previously, were conducted to determine the grid-independent solutions. Throughout the Reynolds number range considered here, the maximum relative error was estimated to be about 2% by comparing the solutions on regular and fine grids with twice of the grid points. Although a few solutions were computed with half the time step to ensure consistency and time-step independence, there was no substantial discrepancy between two different time intervals.

Figure 3 illustrates the experimental apparatus, which consists of blower, chamber, flow measurement system, test section, i.e., rectangular box (200mm X 100mm X 10mm), and flow visualization system. The test section, in which the two diamond-shaped cylinders are installed in side by side arrangement and the inlet and outlet ports are connected for the air to flow in downstream region, is made of acrylic windows for illumination and observation. Mass flow rate of the air, which is flowed from a blower, is measured by an orifice and a manometer. Here the air flow rate is adjusted by a flow valve and a DC inverter connecting the blower. The rectangular box which consists of the fine mesh and a lot of small pipes, is mounted as the inlet section to obtain the uniform velocity profile over the whole cross section.

In measuring the fluid flow velocity profile in the test section, the isothermal air, i.e., no pre-heated air, in which a smoke produced by the device (Porta Smoke Model PS-2001) is added to visualize the fluid flow, is ejected from the injection duct. Illumination which is provided by a light sheet is given to the cross-section. The images of the visualized flow are taken by CCD camera.

An uncertainty analysis [19] yields the following results: the uncertainty for the air flow rate is estimated to be ± 2.5% and that of the time interval measurement is ± 1.0%. Since the uncertainty in the physical properties of less than ± 1% plays only a minor effect on the dimensionless parameter, the average relative uncertainty in Re is estimated to be in the range of ± 3.5% or less.

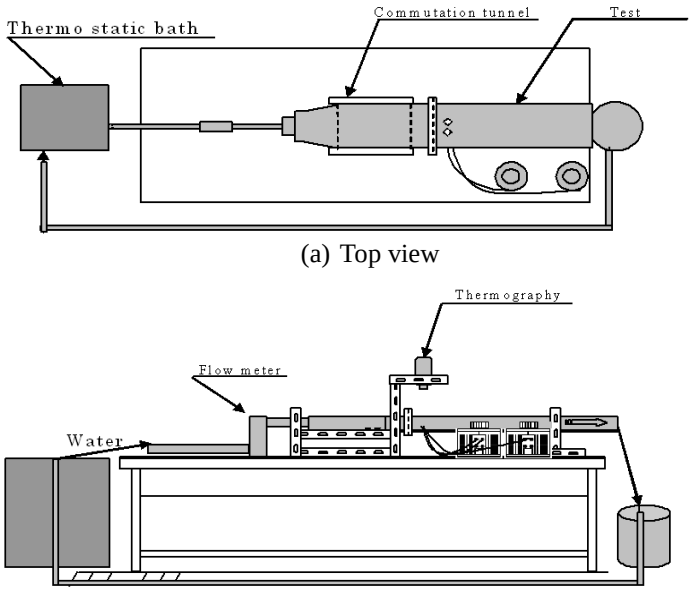

(a) Top view

(b) Side view

FIGURE 3. SCHEMATIC OF EXPERIMENTAL APPARATUS

RESULTS AND DISCUSSION

Side-by-Side Arrangement

As for numerical results and flow pattern obtained by flow visualization method, the velocity vector distribution and digital photograph in the vicinity of the cylinders are shown in the following.

Figure 4(a) depicts instantaneous distribution of fluctuating velocity vectors for s/d = 0.0. Note that a single large Karman vortex is formed behind two diamond-shaped cylinders in the wide range of the Reynolds number. As the gap space yields, the different flow formation behind the twin diamond cylinders causes and is affected by the Reynolds number, as seen in Figs. 4(b)-4(h). For the case of Re = 30 and s/d = 0.5, twin vortex is formed behind the cylinder, while deflection of flow of one side to the other side, i.e., gap-flow and the Karman vortex streets appear in the downstream region behind the other cylinder (Fig. 4(b)). The effect of gap-flow on the gap spacing prevents the substantial evolution of vortex shedding behind a cylinder. As the Reynolds number is increased, Karman vortex in the wake of upper cylinder, gap-flow and extent of fluctuation flow like the heave of waving yield, as seen in Fig. 4(c). It is observed in Fig. 4 that for the gap spacing of s/d = 1.0, 1.5 and 2.0, twin vortex behind upper cylinder and gap-flow are formed in the lower Reynolds number region.

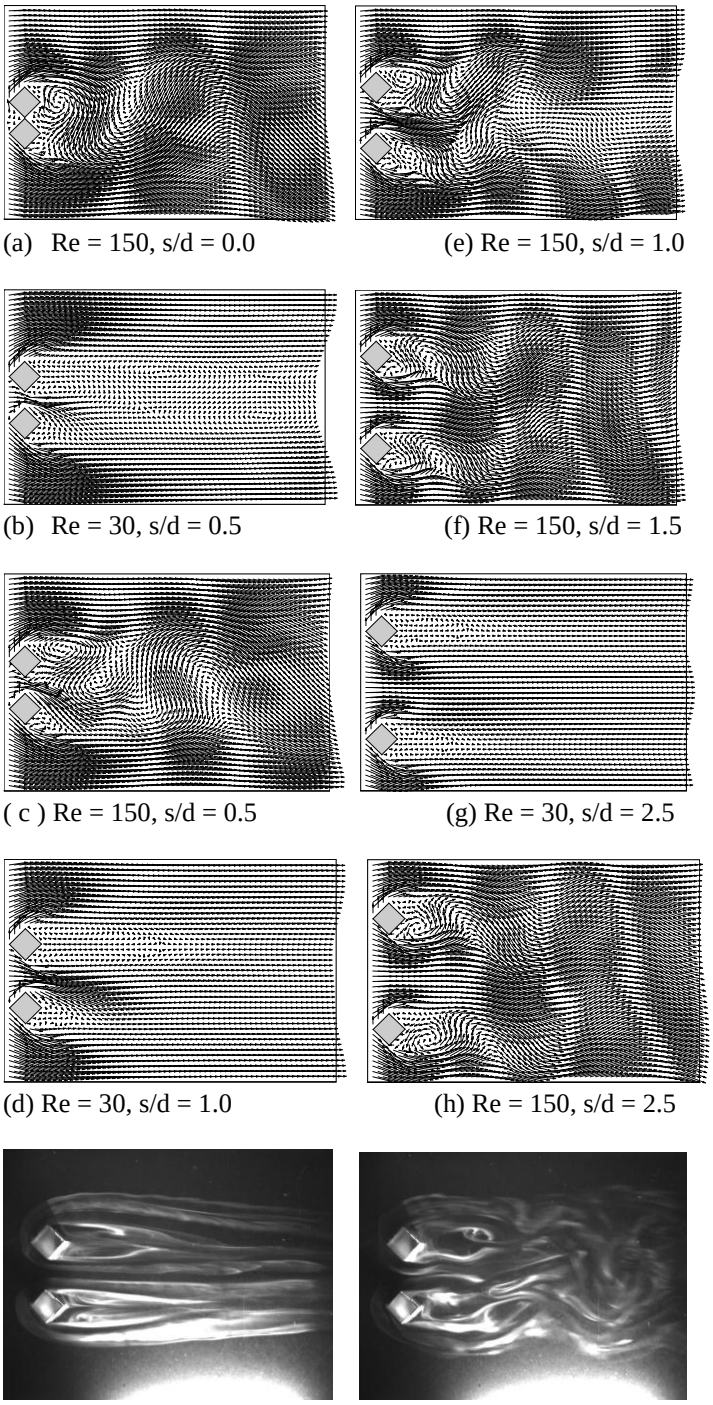

FIGURE 4. PREDICTED VELOCITY VECTOR DISTRIBUTION IN SIDE-BY-SIDE ARRANGEMENT FOR DIFFERENT CONDITIONS AND VISUALIZED FLOW PATTERN

Here, the flow configuration for s/d = 1.0 is alleviated partly retardation by the gap-flow generation in comparison with that for s/d = 0.5. Karman vortex and gap-flow, for s/d = 1.0, are formed with an increase in Re, as seen in Fig. 4(e), while Karman vortex behind upper and lower cylinders yields for s/d = 1.5 in Fig. 4(f). For an additional gap spacing of s/d = 2.5, twin vortex for respective cylinders are formed in the lower Reynolds number region. Furthermore, as the Reynolds number is increased, phase shifting Karman vortex is formed in Fig. 4(h). For comparison, the corresponding flow visualization results at Re=30 and 150 are shown in Figs. 4(i) and (j), respectively. One observes that the flow patters agree with numerical results, as seen in Figs. 4(d) and (e). It is found from the above numerical results that the discriminated flow patterns by numerical flow visualization of velocity vector distribution generated behind two side-by-side diamond-shaped cylinders, depend on both the Reynolds number, Re, and gap spacing, s/d. In order to clarify a few flow patterns which occur at each specific flow condition, the results are symbolized in Fig. 5 in the form of Re versus s/d. Eight different wake patterns are observed over the ranges of Re < 300 and s/d < 2.5 in the present study, as shown in Fig. 5.

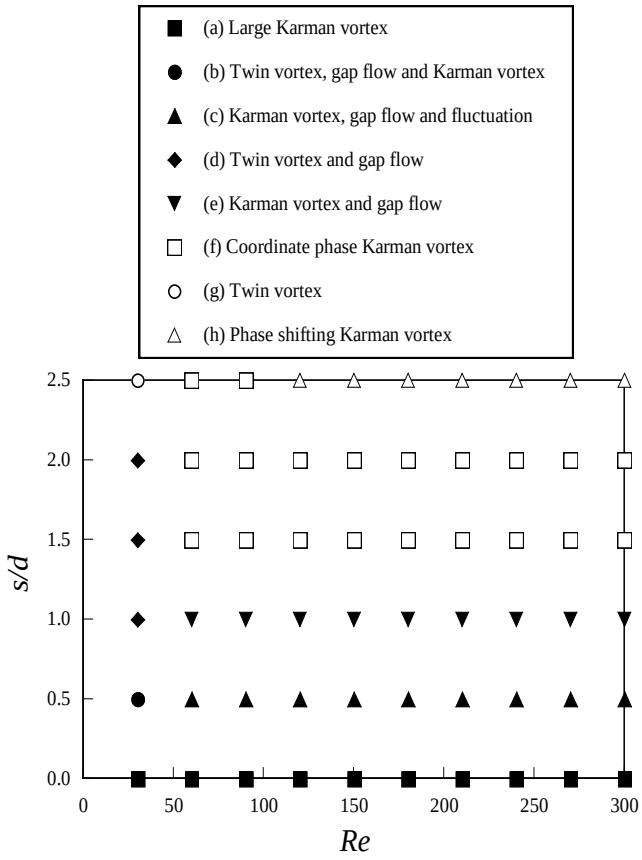

FIGURE 5. PREDICTED FLOW MAP IN SIDE-BY-SIDE ARRANGEMENT FOR DIFFERENT REYNOLDS NUMBER AND s/d OF 0.0 TO 2.5

The flow patterns in the wake region were categorized from flow visualization of velocity vectors distribution, as shown in Fig. 5. As another method, the transition of the flow

pattern regimes is also distinguished by using the time history of the y-axis velocity for different gap spacing. Figure 6(a) depicts the time history of numerical y-axis velocity for the gap spacing of s/d=0.0. Timewise variation of velocity at positions P_3 and P_6 in Fig. 2 indicates the slightly oscillated profile. In the case of Re=30 and s/d=0.5, y-axis velocity denotes a negative value by gap-flow effect as seen in Fig. 6(b), As the Reynolds number is increased, the wave shape of Fig. 6 (c) becomes larger in comparison with Fig. 6(b) and is affected by the vibration of the Karman vortex behind of the cylinders. It is observed in Fig. 6(d) that for the gap spacing of s/d=1.0, the velocity at position P_5 is larger than s/d=0.5. In other words, the gap-flow effect becomes weak in comparison with that at s/d=0.5. At higher Reynolds number, i.e., Re=150, substantial amplification of the oscillation occurs and y-axis velocity and phase of the velocity oscillation at position of P_4 correspond to that at the position of P_6 as the gap-flow effect is almost lost at s/d=1.5. As the result, this vortex shedding configuration forms the same phase, i.e., Karman vortex in the wake of each cylinder. In the case of Re=30 and s/d=2.5 (Fig. 6(g)), y-axis velocity at a diamond-shaped cylinders, i.e., at P_3 and P_4 is the almost same as them at the position of P_5 and P_6. For a gap spacing of s/d=2.5, the wake behind each cylinder is independently formed. However, phase shifting occurs at positions of P_4 and P_6 in comparison with that at s/d=1.5. Vortex shedding formation of Karman vortex is formed for each cylinder.

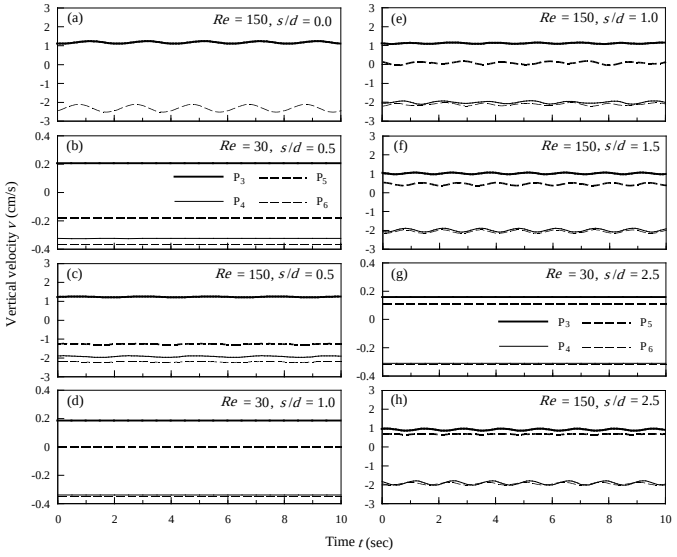

FIGURE 6. TIME HISTORY OF PREDICTED Y-AXIS VELOCITY IN SIDE-BY-SIDE ARRANGEMENT FOR VARIOUS REYNOLDS NUMBERS AND s/d

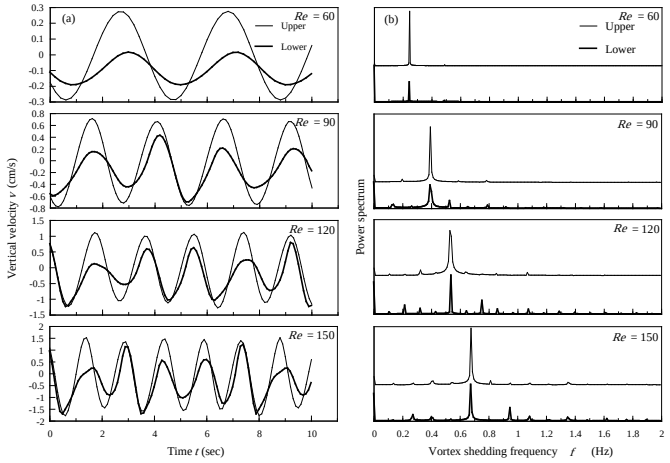

FIGURE 7. POWER SPECTRUM OF PREDICTED Y-AXIS VELOCITY OSCILLATION IN SIDE-BY-SIDE ARRANGEMENT AT POSITION P1 AND P2 FOR Re=60-150 AND s/d=1.0

In order to make the fluid flow characteristics of vortices behind two diamond-shaped cylinders in side-by-side arrangement clearer, power spectrum obtained from periodical vertical velocity at s/d = 1.0 is shown in Fig. 7 with different Reynolds numbers, as the parameter. For reference, the corresponding time-history of predicted y-axis velocity is also depicted in Fig. 7. One observes that as the Reynolds number increases, the peak value of the power spectrum and the corresponding vortex shedding frequency are amplified. In other words, the generations of Karman vortex streets behind the cylinders are intensified with an increase in the Reynolds number.

An attempt is made to the effect of gap spacing on the vortex-shedding frequency. Based on the numerical results, the frequency, f, of the vortex generated behind two side-by-side cylinders is plotted in Fig. 8 in the form of Strouhal number Sr versus Reynolds number Re with s/d, as the parameter. Here, the Strouhal number, St, is defined using width of diamond-shaped island, d, axial mean velocity of the main flow, Uo and frequency f which corresponds to the peak of the power spectrum of the vertical velocity oscillation, as seen in Fig. 7. One observes that (i) for s/d = 0, the eddy shedding frequency is increased with an increase in the Reynolds number and the asymptotic behavior appears in the larger Reynolds number region, (ii) in contrast, non-periodic vortex, for different s/d, occurs behind the cylinder less than Re = 30, and (iii) as the Reynolds number is increased, vortex shedding causes and the Strouhal number is nearly constant for the Reynolds number of 90 to 300. Note that although the Strouhal number of a single diamond cylinder is comparable to that for a pair of cylinders arranged side-by-side for the wide range of the Reynolds number, the eddy shedding frequency is affected by the gap spacing s/d.

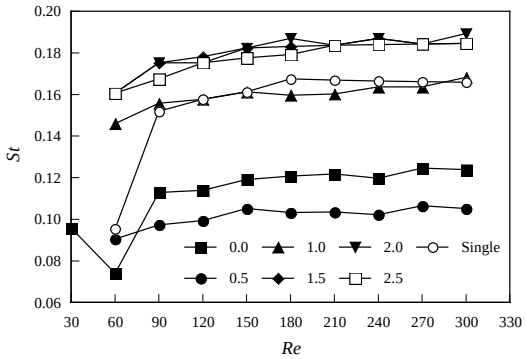

FIGURE 8. PREDICTED STROUHAL NUMBER IN SIDE-BYSIDE ARRANGEMENT FOR Re and s/d

Tandem Arrangement

Mizushima and Suehiro [20] investigated the flow past two circular cylinders arranged in tandem and reported that symmetric flow appears with respect to the x axis through the centers of the circular cylinder at small Reynolds number for every value of the spacing between two cylinders. In contrast, the steady symmetric or unsteady axisymmetric flow past two diamond cylinders occurs at lower Reynolds number and at small ratio, s/d, of cylinder separation distance to size of diamond-shaped cylinder, as seen in the following.

Figures 9(a) and (c), for Re=30, depict snapshots of the flow pattern for two cases of s/d=0.0 and 1.0, respectively. Note that for fixed Re, the map is classified for two cases for the wide range of s/d, as shown in Fig. 10. Here, Fig. 10 illustrates the flow map past two diamond-shaped cylinders arranged in tandem. The structure of the flow in free stream changes with the cylinder separation distance, s/d. In the other words, for the case with s/d=0.0, the flow is steady and twin vortexes are constructed behind the downstream cylinder, that is the flow behind the downstream cylinder has a recirculation zone, as seen in Fig. 9(a). As s/d is increased, the flow behind the upstream cylinder becomes unsteady and twin vortexes disappear, as seen in Fig. 9(c). One observes that behind the upstream cylinder a sequence of alternating crossing of flow streaklines from one side of the cylinder to the other through the spacing between both cylinders takes place, but the flow past the downstream cylinder is not disturbed due to an alternating change in the flow direction in the spacing. As the Reynolds number is increased, the other fluid flow phenomena, which depend on the cylinder separation distance, s/d, yield, as seen in Figs. 9 and 10. Figure 9 (b), for Re=150 and s/d=0.0, observes that twin vortex which is similar to that of a single cylinder, appears behind the rear diamond cylinder. This flow patter is affected with an increase in s/d (Fig. 9(d)). Figure 9(d) shows the snapshot of the flow pattern for s/d=1.0. It is observed that the alternating change in the flow direction, i.e., oscillatory fluid motion takes place in the gap between the two circular cylinders, that is, a vortex generated behind the downstream diamond cylinder, i.e., vortex shedding occurs in unsymmetrical with respect to the x axis. For an additional gap spacing of s/d = 3.5 and Re = 210 in Fig. 9(e), narrow Karman vortex in the wake for each cylinder is formed in the moderate gap spacing. As the Reynolds number is increased, wide Karman vortex that downstream cylinder is enveloped by a vortex shedding in the upstream wake, is formed so as to pass through wake transition region of Karman vortex streets, as shown in Fig. 9(f).

Throughout Figs. 9 and 10, the flow pattern generated behind two tandem cylinders depends on both Reynolds number and gap spacing. Six kinds of wake pattern are observed over the ranges of Re < 300 and s/d < 5.0 in the present study. The flow patterns in the wake region of the diamond-shaped islands, for the large Reynolds number region, are affected by s/d.

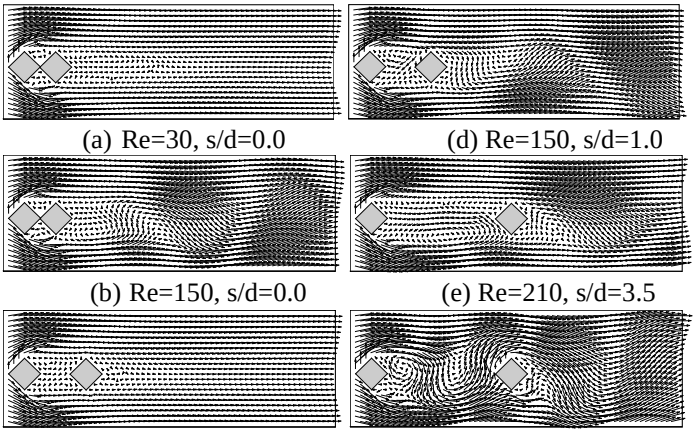

FIGURE 9. PREDICTED VELOCITY VECTOR DISTRIBUTION IN TANDEM ARRANGEMENT FOR CATEGORIZED REGIMES

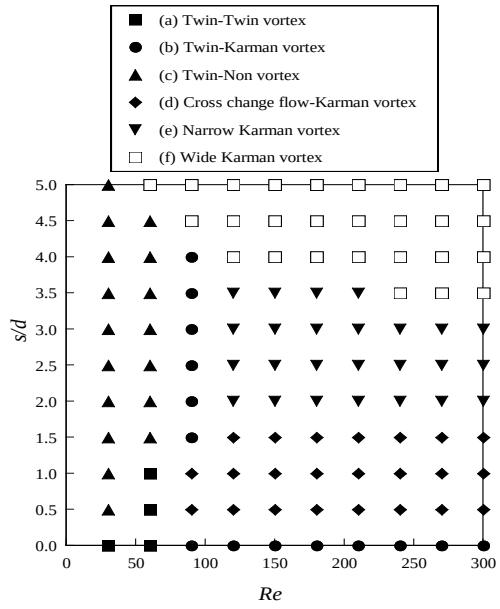

FIGURE 10. PREDICTED FLOW MAP IN TANDEM ARRANGEMENT FOR VARIOUS REYNOLDS NUMBERS AND s/d

The transition of the flow pattern regimes is confirmed using a time history of the predicted y-axis velocity for various gap spaces, as shown in Fig. 11. Figure 11 is illustrated in the same form as Fig. 6. Figure 11(a) depicts fluctuating vertical velocity at four different positions for the gap spacing of s/d = 0.0. y-axis velocity at positions P3 and P6 of downstream cylinder indicates non-fluctuation in vertical streamwise direction. As the Reynolds number is increased, y-axis velocity slightly oscillates in comparison with Fig. 11(a), as shown in Fig. 11(b). This is because Karman vortex generation behind the cylinders is stimulated with an increase in the Reynolds number. This tendency becomes larger for s/d=1.0, as seen in Fig. 11(d). As the gap spacing is widened in s/d=3.5, y-axis velocity oscillation appears at positions P5 and P6 in the wake of downstream cylinder which at positions P5 and P6 is affected by the vortex shedding discharged behind upstream cylinder. As the Reynolds number is increased at Re=240, amplitude of timewise variation of y-axis velocity is substantially enhanced for each position expressed magnitude of fluctuation (Fig. 11(f)). The flow transition region and flow phenomenon in the wake of cylinders are categorized by utilizing time history of y-axis velocity.

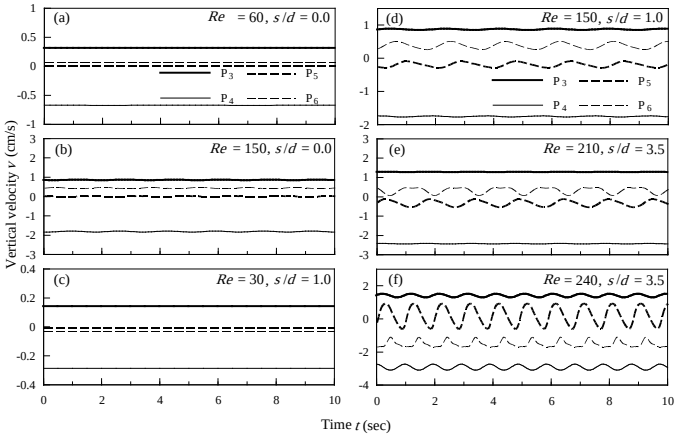

FIGURE 11. TIME HISTORY OF PREDICTED Y-AXIS VELOCITY IN TANDEM ARRANGEMENT

The frequency characteristic of the wake over two diamond-shaped cylinders in tandem arrangement is calculated from periodical variation of y-axis velocity for various different Reynolds numbers at s/d = 3.5. Figure 12 depicts power spectrum from timewise variation of predicted vertical velocity at positions P_1 and P_2. The vortex shedding frequency that the peak value of the power spectrum shows, is amplified with an increase in the Reynolds number. The vortex shedding frequency of the peak value behind upstream cylinder at position P_1 indicates the same peak of downstream cylinder at P_2, but the amplitude peak of vortex shedding frequency and the amplitude of power of power spectrum at P_1 are smaller than at P_2 for Re<210. However, the spectrums at P_1 and P_2 are the same value over Re = 240.

Using the frequency of the peak power spectrum of the y-axis velocity at positions P_1 and P_2, the Strouhal number is obtained. The predicted Strouhal number is summarized in Fig. 13 in the same form as Fig. 8. One observes that the Strouhal number is increased with an increase in the Reynolds number and the asymptotic behavior appears in the larger Reynolds number region. In the case of s/d<3.5, St is gradually decreased with an increase in gap spacing. However, St, for 3.5<s/d, is increased with an increase in s/d and gradually approaches the value of a single diamond-shaped cylinder. Thus, the traditional region that St is increased with an increase in the Reynolds number, exists in the wake behind tandem diamond-shaped cylinders, i.e., for s/d<3.5.

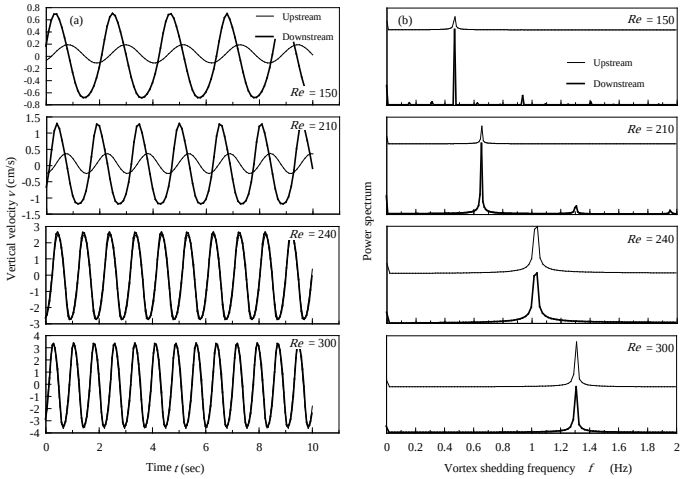

FIGURE 12. TIME-HISTORY OF Y-AXIS VELOCITY AND POWER SPECTRUM AT P1 AND P2 IN TANDEM ARRANGEMENT Re = 150, 210, 240, 300 and s/d = 3.5.

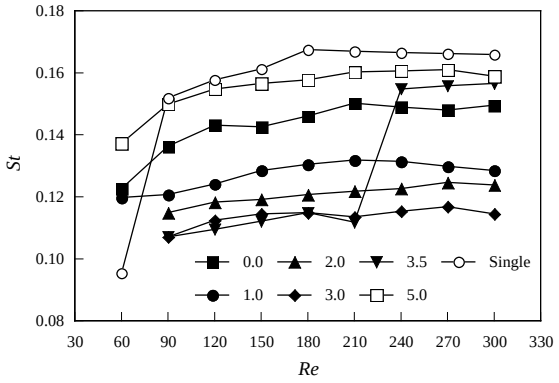

FIGURE 13. PREDICTED STROUHAL NUMBER IN TANDEM ARRANGEMENT FOR Re and s/d

CONCLUSIONS

In this study, numerical and experimental study has been performed on fluid flow phenomenon around a pair of diamond-shaped cylinders arranged in side-by-side and tandem in free stream. Velocity characteristics behind two diamond-shaped cylinders are dominated by Reynolds number and gap spacing. The study discloses that:

(i) The generations of Karman vortex streets behind the diamond-shaped cylinders are intensified with an increase in the Reynolds number.

(ii) The categorized flow patterns in the wake region of the diamond-shaped islands are affected by s/d in high Reynolds number region, that is as the gap spacing increases, the vortex shedding frequency decrease for each cylinder arrangement.

(iii) The vortex shedding frequency in the wake of diamond-shaped cylinders depends on the gap spacing and this trend becomes lager with an increase in Reynolds number. Note that the vortex shedding frequency approaches gradually that of the single cylinder.

NOMENCLATURE

B	computational domain in x direction
d	diamond size in y direction, m
f	vortex shedding frequency, Hz
l	diamond size in x direction, m
P	pressure, Pa
Re	Reynolds number, $U_0 d/\nu$
s	separation distance between a pair of diamonds, m
St	Strouhal number, fd/U_0
t	time, sec
u	velocity component in x direction, m/s
U_0	uniform inlet velocity, m/s
v	velocity component in y direction, m/s
W	computational domain in y direction
Δ	difference
θ	aspect upstream apex angle in diamond, degree
ν	kinematical viscosity, m^2/s
ρ	density, kg/m^3

REFERENCES

[1] Yu, D. and Kareem, A., 1998, "Parametric study of flow around rectangular prisms using LES", *Journal of Wind Engineering and Industrial Aerodynamics* **77**, pp. 653-662.

[2] Kahawita, R. and Wang, P., 2002, "Numerical simulation of the wake flow behind trapezoidal bluff bodies", *Computer & Fluid*, **31**, pp. 99-112.

[3] Agrawal, a., Djenidi, L. and Antonia, R.A., 2006, "Investigation of the flow around a pair of side-by-side square cylinders using the lattice Boltzmann method", *Computer & Fluid*, **35**, pp. 1093-1107.

[4] Valencia, A. and Paredes, R., 2003, "Laminar flow and heat transfer in confined channel flow past square bars arranged side by side", *Int. J. Heat and Mass Transfer*, **39**, pp. 721-728.

[5] Wang, Z. J. and Zhou, Y., 2005, "Vortex interactions in a two side-by-side cylinder near-wake", *International Journal of Heat and Fluid Flow*, **26**, pp. 362-377.

[6] Akilli, H., Akar, A. and Karakus, C., 2004, "Flow characteristics of circular cylinders arranged side-by-side in shallow water", *Flow Measurement and Instrumentation*, **15**, pp. 187-197.

[7] Miau, J. J., Wang, H. B. and Chou, J. H., 1996, "Flopping phenomenon of flow behind two plates placed side-by-side normal to the flow direction", *Fluid Dynamics Research*, **17**, pp. 311-328.

[8] Wei, C. Y. and Chang, J. R., 2002, "Wake and base-bleed flow downstream of bluff bodies with different geometry", *Experimental Thermal and Fluid Science*, **26**, pp. 39-52.

[9] Ohya, Y., Okajima A. and Hayashi, M., 1989, "Interference and vortex shedding, Aerodynamics and Compressible Flow", Vol. 8, Gulf Publishing Company, Huston, TX, pp. 322-389.

[10] Ohmi, K. and Imaichi, K., 1992, "Vortex wake visualization of two circular cylinders", in Proceedings of 6th International Symposium of Flow Visualization, pp. 322-326.

[11] Eissler, W., Drtina, P. and Frohn, A., 1992, "Cellular automata simulation of flow around chains of cylinders", *Int. J. Numerical Methods Fluids*, **34**, pp. 773-785.

[12] Mittal, S., Kumar, V. and Reghuvanshi, A., 1997, "Unsteady incompressible flows past two cylinders in tandem and staggered arrangement", *Int. J. Numerical Methods Fluids*, **25**, pp. 1315-1324.

[13] Meneghini, J.R., Saltara, F., Siqueira, C. L. R., and Ferrari, Jr. J. A., 2001, "Numerical simulation of flow interference between two circular cylinders in tandem and side-by-side arrangement", *J. Fluids Structure*, **15**, pp. 327-335.

[14] Sharman, B., Lien, F.S., Davidson, L. and Norberg, C., 2005, "Numerical prediction of low Reynolds number flows over two tandem circular cylinders", *Int. J. Numerical Methods Fluids*, **47**, pp. 423-433.

[15] Carmo, B. S. and Meneghini, J. R., 2006, "Numerical investigation of the flow around two circular cylinders in tandem", *Journal of Fluids and Structures*, **22,** pp. 979-988.

[16] Umeda, S. Yang, W. J. and Kanbara, H., 2001, "Characteristics of wake flows behind a diamond-shaped cylinder", *Transactions of the Visualization Society of Japan*, **21**, pp. 58-64.

[17] Harlow, F. H., and Welch, E. J., 1965, "Numerical Calculation of Time-Dependent Viscous Incompressible Flow of Fluid with Free Surface", *Phys. Fluids*, **8,** pp. 2182-2189.

[18] Hirt, C. W., Nichols, B. D., and Romero, N. C., 1975, SOLA-A Numerical Solution Algorithm for Transient Fluid Flows, *LASL Report*, LA-5852.

[19] Kline, S.J. and McClintock, F.A., 1953, "Describing Uncertainties in Single-Sample Experiments", *Mechanical Engineering*, pp. 75-76.

[20] Mizushima, J. and Suehiro, N., 2005, "Instability and transition of flow past two tandem circular cylinders", *Physics of Fluids*, **17**, pp. 1-11.